Fragmentation Dynamics of Size-Selected Pyrrole Clusters Prepared by Electron Impact Ionization: Forming a Solvated Dimer Ion Core †

ARTICLE *in* THE JOURNAL OF PHYSICAL CHEMISTRY A · JANUARY 2008

Impact Factor: 2.69 · DOI: 10.1021/jp0751561 · Source: PubMed

Fragmentation Dynamics of Size-Selected Pyrrole Clusters Prepared by Electron Impact Ionization: Forming a Solvated Dimer Ion Core†

Václav Profant, Viktoriya Poterya, and Michal Fárník*

J. Heyrovský Institute of Physical Chemistry, Academy of Sciences of the Czech Republic, Prague 8, Czech Republic

Petr Slavíček‡

Department of Physical Chemistry, Institute of Chemical Technology, Technická 5, Prague 6, Czech Republic

Udo Buck

Max-Planck-Institut für Dynamik und Selbstorganization, Bunsenstrasse 10, D-37073 Göttingen, Germany

Received: July 3, 2007; In Final Form: August 2, 2007

Structure and dynamics of size-selected charged pyrrole clusters have been studied by means of molecular beam scattering experiments and ab initio calculations. Small neutral Py_n clusters were produced in Py/He mixture expansions, and the scattering experiment with a secondary beam of He-atoms was exploited to select the neutral clusters of different sizes. The complete size-selected fragmentation patterns for the neutral dimer to the tetramer after an electron impact ionization at 70 eV were obtained from the measurements of the angular and velocity distributions at different fragment masses. All the investigated cluster sizes decay mainly to the monomer ions Py_1^+ (from 60 to 80% of the corresponding neutral size) and to the dimer ion Py_2^+ (20−30%). The trimer ions Py_3^+ are generated to less than 10% from the neutral trimer and tetramer. To explain the observed results, we have calculated the structures and energetics of pyrrole clusters up to the trimer for the neutral and the ionic state using DFT and PMP2 methods. The ab initio calculations show that ionized pyrrole clusters are formed with a dimeric core that is solvated by neutral pyrrole molecules. In addition, the ground and ionic state of Py−Ar complexes were calculated at CCSD(T) level with extended basis in relevance to the mixed clusters produced in supersonic expansions of Py seeded in Ar. The calculated dissociation energies of the Py−Ar and $(Py-Ar)^+$ complexes indicate that Ar atoms are able to rapidly evaporate after ionization. The combined analysis of the fragmentation probabilities, and calculations allowed us to estimate the distribution of energy deposited in the clusters after the electron impact, which peaks above 1 eV and has a tail up to 5 eV.

1. Introduction

Gas-phase molecular clusters represent an essential model for understanding the fundamental aspects of intermolecular interactions.[1] The size of the clusters can be gradually changed, adding complexity to the system. Molecular clusters composed of aromatic molecules belong to the most important ones. Noncovalent interactions between aromatic molecules are of primary importance for such phenomena as nucleic acid base−base interaction, self-assembled structures, or protein architecture. Among the aromatic clusters, the most studied systems are composed of benzene. Such clusters represent prototypical systems for studying $\pi-\pi$ and $X-H\cdots\pi$ interactions. Benzene clusters have been studied thoroughly using various experimental and theoretical techniques both in the ground state,[2] in the excited states,[3] and upon ionization.[4]

Molecular clusters of pyrrole C_4H_5N (Py), on the other hand, have been explored to a much lesser extent. Pyrrole is one of the simplest heterocyclic molecules, and it is an important prototype of heteroaromatic compounds forming the molecular basis of life, i.e., nucleobases. Pyrrole units are present in many biological molecules, e.g., in hemes, chlorophylls, or in vitamin B_{12}. The ground state pyrrole dimer has been investigated by rotational spectroscopy[5] and by ab initio calculations.[6−8] While the benzene dimer has two very closely lying minima (T-shaped and parallel displaced structure), the pyrrole dimer was found to form only one minimum with an approximately T-shape structure with an angle 55.4° between the two units, forming a $N-H\cdots\pi$ hydrogen bond. More recently, larger pyrrole clusters have been characterized by FTIR spectroscopy and by DFT calculations.[9] These studies have shown that pyrrole clusters in the ground state form cyclic structures.

Isolated pyrrole molecules have been also studied in the excited states[10−17] and after ionization.[18] The interest in the excited pyrrole molecule results again from its importance as a building block of biological molecules. Indeed, detailed knowledge of the processes following UV absorption or ionization is essential for the understanding of radiative and oxidative DNA damage.[19,20] Surprisingly, to our best knowledge, pyrrole molecular clusters have not been studied in excited and ionic

† Part of the "Giacinto Scoles Festschrift".

* Corresponding authors. E-mail: michal.farnik@jh-inst.cas.cz (M.F.); Petr.Slavicek@vscht.cz (P.S.).

‡ Also at: J. Heyrovský Institute of Physical Chemistry, Academy of Sciences of the Czech Republic, Prague 8, Czech Republic.

10.1021/jp0751561 CCC: $37.00
Published on Web 10/11/2007

states. The photodissociation dynamics of the size-selected pyrrole clusters has recently been studied in our laboratory.[21] Also the group of Kitsopoulos has recently reported a study of photodissociation and resonance-enhanced multiphoton ionization of Py molecules clustered with Xe atoms.[22]

The purpose of this work is to explore the dynamical behavior of the pyrrole clusters upon electron impact ionization such as cluster fragmentation and to gain understanding of the nature of bonding in charged pyrrole clusters. As a byproduct of this study, the cluster size distributions corresponding to the different expansion conditions were obtained. In this work, we combine molecular beam scattering experiments with electronic structure calculations on several levels of theory. Experiment and theory provide complementary information here. While the experiment can deliver fragmentation probabilities of size-selected clusters, ab initio calculations yield the energetics of the induced dynamical processes and also the structures of the involved species. We have theoretically studied pyrrole complexes both in the ground and in the ionized states using density functional and MP2 techniques.

It is instructive to compare the behavior of pyrrole clusters with benzene clusters. As we already have pointed out, the benzene dimer has multiple minima on its potential energy surface. The global minimum corresponds to a T-shape structure.[23] There has been some controversy about the nature of cluster radical cations. However, the general agreement seems to be that the ionic dimer core is surrounded by remaining benzene molecules. This conclusion is based on a large variety of experimental results[24−26] as well as on different ab initio calculations ranging from the Hartree−Fock method with a small basis[27] to DFT,[4] CASSCF, and MRCI[28] to CCSD(T) methods.[29] Apart from benzene clusters, also other aromatic systems have been studied, e.g., naphthalene clusters[30] or benzene−indole clusters.[31]

Experimentally, the clusters are prepared by expansions in helium or argon carrier gas. While the production of clusters of helium with aromatic molecules is improbable under our experimental conditions,[32] the interaction of argon atoms with pyrrole can be important for interpreting the experimental findings. We have therefore also investigated complexes of pyrrole with argon by means of electronic structure calculations. Calculations have been performed both for the ground state as well as for the ionized state. Because ground-state complexes between rare gases and aromatic molecules are bound mostly by dispersion interaction, we have employed MP2 and CCSD-(T) methods with larger basis sets for their description. Similarly as for pyrrole clusters, even for pyrrole−argon clusters there exists only some (experimental) information about the ground state[34] while no information is available for the ionized state. On the other hand, benzene−argon complexes have been addressed both experimentally and theoretically in the ground and ionized states.[35−37]

In the following section, we briefly describe the scattering experiment and the data analysis procedure. Then the results of the experiment will be presented, and the fragmentation probabilities for various neutral cluster sizes will be derived. In the following sections, the electronic structure calculations will be introduced and the experimental results discussed based on these calculations. Finally, conclusions will be drawn.

2. Experimental and Theoretical Methods

A. Experiment. The schematic picture of the experimental apparatus is shown in Figure 1. It was previously used in the Max-Planck Institute in Göttingen for both the scattering experiments[38] and the photodissociation of molecules in clusters.[39] Recently, the equipment has newly been installed at the J. Heyrovský Institute of Physical Chemistry in Prague. The details of the experiment can be found in earlier publications from Göttingen.[39,40]

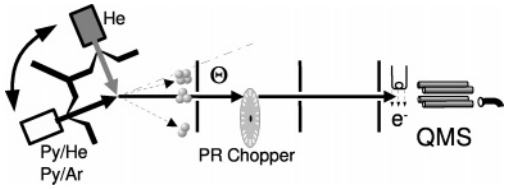

Figure 1. Schematic view of the experimental apparatus.

TABLE 1: Experimental Conditions

	cluster beam		secondary beam
gas	Py/He	Py/Ar	He
nozzle diameter (μm)	60	60	30
conical nozzle angle (deg)	30	30	
expansion pressure p_0 (bar)	1.5	3.0	30
nozzle temperature T_0 (°C)	9	9	35
pyrrole reservoir temperature T_R (°C)	8	8	
pyrrole concentration (%)	0.33	0.16	
mean cluster size $\bar{n}$	3	12[a]	
cluster velocity (ms^{-1})	1525	509	1753
speed ratio	25	29	42

[a] The mean cluster size $\bar{n}$ here means the total size ($\bar{m} + \bar{n}$) of the mixed Ar_mPy_n clusters produced in Ar expansions.

The cluster beam was produced by a supersonic expansion of pyrrole vapor seeded in He or Ar buffer gas through a conical nozzle of 60 μm diameter, 2 mm long, and 30° opening angle. The pyrrole (98 %, Aldrich) was filled into a reservoir[41] outside the vacuum chamber, which was kept in a thermal bath at a constant temperature $T_R = 8°$. The buffer gas carried the pyrrole molecules to the nozzle kept at a slightly higher temperature $T_0 = 9°$ to prevent pyrrole condensation in the nozzle. The present expansion conditions are summarized in Table 1.

Helium was expanded through a 30 μm pinhole nozzle at room temperature and 30 bar pressure to produce the secondary beam. After passing through skimmers, the two molecular beams were intersected mutually perpendicular in a differentially pumped scattering chamber. The two vacuum chambers hosting the beam sources were attached to the scattering chamber so that the whole assembly connected with a flexible bellows to the next chamber could be rotated in the horizontal plane. Turning to a given laboratory angle Θ allowed the clusters scattered to this particular angle to continue along the apparatus axis to the detector (see Figure 1). The scattered clusters entered a vacuum chamber hosting a pseudorandom chopper for measuring their time-of-flight (TOF) distributions. Then after passing another vacuum chamber used in the photodissociation experiments,[21] they arrived in the detector chamber, where they were ionized by an impact of 70 eV electrons and the fragments were analyzed with a quadrupole mass spectrometer and detected by an electron multiplier.

The scattering analysis enables us to find a unique correlation between detected cluster ions and their neutral precursors independent of the cluster size distribution in the primary beam and the fragmentation process in the ion source.[42] The method relies on the specific kinematic behavior of clusters with different sizes scattered from a target beam illustrated by the Newton diagram in Figure 2. The vectors in the velocity space denote cluster beam velocity $\vec{v}_c$, He beam velocity $\vec{v}_{He}$, collision velocity $\vec{g}$, and the velocity $\vec{c}_1$ with which the center-of-mass

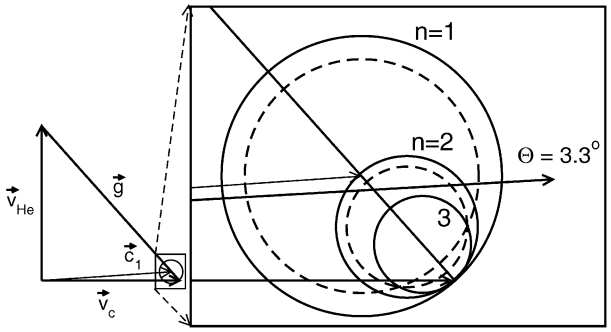

Figure 2. Newton diagram for collisions of pyrrole clusters produced in He expansions with a perpendicular beam of He atoms (see the text for details).

(CM) of the system (pyrrole molecule−helium atom) moves. The elastically scattered molecules can be found in the velocity space on the full circle ($n = 1$) with the center at the end of $\vec{c}_1$ vector. For the Py_n clusters, the CM velocity changes with n, and correspondingly the center of the scattering circle shifts and the radius becomes smaller for larger n, as is illustrated for $n = 2$ and 3 in Figure 2. The dashed circles correspond to the scattering with 30% energy transfer (see the experimental results below). Thus under the typical experimental conditions with a moderate energy transfer in the collision, each Py_n cluster could be scattered into the laboratory (LAB) system only within a certain angular range. The tangent to the corresponding circle determines the threshold LAB scattering angle Θ_n to which the particular cluster of size n can maximally be deflected. Setting the detector to a larger scattering angle $\Theta > \Theta_n$ implies that only clusters smaller than n can reach the detector.

The neutral clusters of different sizes n deflected to a LAB angle Θ arrive at the detector with different laboratory velocities v_f (see Figure 2). Therefore the cluster TOF distributions were measured for various cluster fragment masses at particular scattering angles Θ using the pseudorandom chopper and recording the arrival times at the detector. This allowed us to disentangle the contributions from the various neutral cluster sizes to the given ionic fragment. The signal of the cluster fragment Py_k^+ of the size k originating from the neutral cluster Py_n of the size n scattered to the LAB angle Θ is given by

$$N_{nk}(\Theta, v_f) = K\rho_n\sigma_n(\Theta)C_n f_{nk} \quad (1)$$

where ρ_n is the density of clusters of size n in the beam, σ_n is the differential scattering cross section with the target beam in the LAB system, C_n the total ionization cross section, f_{nk} the probability for the formation of an ion of size k from a cluster of size n, and the constant K contains the other scattering characteristics not relevant to the cluster size separation. From the distributions $N_{nk}(\Theta)$, measured at the different laboratory angles for the different cluster fragments Py_k^+, the fragmentation probabilities f_{nk} could be obtained by an analysis described in more detail elsewhere.[42,43]

B. Theoretical Calculations. We have performed ab initio calculations to gain further insight into the behavior of the pyrrole clusters after the ionization. In particular, we have calculated the structure and energetics of the pyrrole monomer, dimer, and trimer in their neutral form and after ionization. There are three major sources of problems in the calculations of open shell van der Waals complexes. First, correlation energy has to be included. Density functional theory based methods and MP2 calculations usually represent a good compromise for a system of this size. Second, the one electron basis should be sufficiently saturated. The problem of the one electron basis is for van der Waals complexes specifically manifested by the basis set superposition error (BSSE). As discussed later, the inclusion of the BSSE for open-shell complexes with two units of the same type is not straightforward. The last problem to be addressed is what sort of electronic wavefunction has to be utilized for the open-shell system description. Unrestricted formalism suffers from the inclusion of the higher spin states. It can thus be utilized only if the spin contamination is sufficiently small. We have used the unrestricted version of MP2 and DFT methods with a subsequent annihilation of the higher spin components for the optimized geometry[46] (PMP2 method). The spin contamination in all cases under study was reasonably low (S^2 is typically below 0.8 for radical cations), and we can thus safely apply the above scheme. It was shown that the spin projection procedure significantly improves the calculated ionization potentials.[47] The ground-state structures have been optimized at the DFT/B3LYP and MP2 levels using a 6-31+g* basis. Because the complexes under study are bound dominantly by electrostatic interactions, this basis set is adequate even for the description of nonbonding interactions. The MP2 and DFT methods combined with this basis provide a reasonable description of the ground-state complexes, and it can therefore be used for the calculation of the corresponding radical ions. Note also that all the results obtained with the 6-31+g* basis are reasonably close to those obtained with a smaller 6-31g* basis.

Larger pyrrole clusters were prepared in co-expansion with argon. To discuss the possible clustering of argon atoms with pyrrole clusters we have also performed electronic structure calculations of the pyrrole−argon neutral cluster and the cation. Pyrrole−argon clusters are bound dominantly by the dispersion interaction and to a lesser extent by the induction interaction. The DFT approach in this case is not adequate and we have thus studied this system by MP2 and CCSD(T) methods. Also the one electron basis has to be saturated to larger degree, and an aug-cc-pVDZ basis augmented with a set of midbond functions has thus been utilized.

All the calculations have been performed using the Gaussian03 program suite.[48]

Note at this point that estimating basis set superposition error for the pyrrole dimer and pyrrole trimer radical cations is more difficult than for the neutral species. The counterpoise correction of Boys and Bernardi[49] cannot be directly used. For this correction, the system has to be divided into two subunits A and B. It is considered that subunits A and B do not change their chemical nature in the course of complexation. This is not the case for a pyrrole dimer. Here, the positive charge is delocalized over the two subunits for the complex while it is localized on one of the subunits in the dissociation limit. The corresponding A or B species in the complex has thus no counterpart as an isolated molecules. The problem can be visualized by considering the pyrrole dimer cation in the ground-state optimal geometry. One can calculate the basis set superposition correction by assuming that the charge is localized on a pyrrole unit with a free hydrogen. Then this quantity is 0.017 eV. One can also assume the charge being localized on the a hydrogen-bonded pyrrole subunit. BSSE correction is then 0.020 eV. While the difference between the two quantities is not huge, they can provide at least an order-of-magnitude estimate of the importance of the BSSE effects. The estimate of BSSE for a dissociation of a trimer complex is more reliable because the charge is localized on the dimer core in this case. Counterpoise correction of the basis set superposition error is of course not the only method for how to deal with a basis set

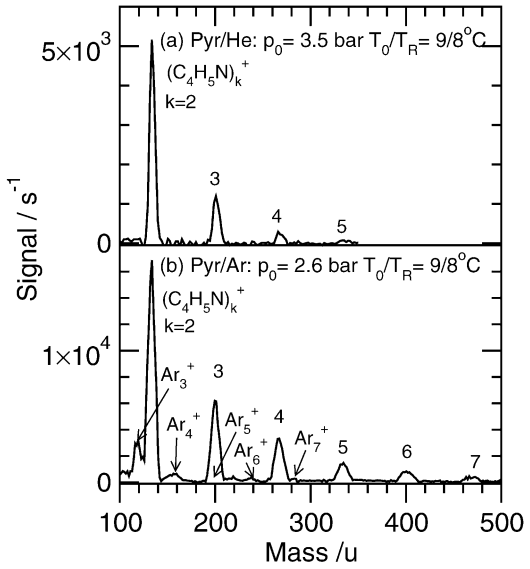

Figure 3. Mass spectra measured in expansion of pyrrole in (a) He buffer gas and (b) Ar buffer gas. The expansion conditions are given at the top and mass peaks corresponding to the various Py_k^+ fragment sizes k are indicated. In the Ar expansions, a weak progression of the Ar_n^+ peaks is observed.

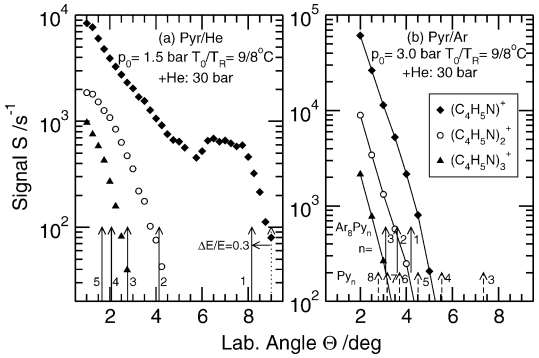

Figure 4. Measured angular distributions for pyrrole clusters in collisions with He atoms. The clusters were produced in expansion with (a) He buffer gas and (b) Ar buffer gas, and the distributions were measured for fragment ion masses of monomer Py^+ (black diamonds), dimers Py_2^+ (open circles), and trimers Py_3^+ (black triangles). The lines in (b) connect the experimental points for better clarity. The arrows indicate the positions of the threshold angles for neutral clusters as discussed in the text in more detail.

superposition error; one can, for example, perform a basis set extrapolation. This is, however, much more demanding and going beyond the scope of this paper.

3. Experimental Results

Figure 3 shows the mass spectra measured in the expansion of pyrrole in (a) He-buffer gas and (b) Ar-buffer gas. The expansion conditions are given at the top and mass peaks corresponding to the Py_k^+ fragments are labeled by k. In the He expansion, only the mass peaks corresponding to the Py_k^+ ions are significantly populated. In the Ar expansion, besides the larger Py_k^+ fragments, also a weak progression of the Ar_m^+ cluster peaks is noticeable. Although it partly overlaps with the pyrrole cluster ions, the two progressions could be disentangled by careful comparison to the pure Ar expansions.

Figure 4 shows the measured angular distributions $S_k(\Theta)$ for pyrrole clusters in collisions with He atoms. The left panel (a) shows the angular distributions for clusters produced in He expansions. The measurements were done for the mass of the monomer ion Py^+ (black diamonds), the dimer ion Py_2^+ (open circles), and the trimer ion Py_3^+ (black triangles). The arrows at the bottom correspond to the positions of the threshold angles for the neutral clusters of the indicated sizes. The threshold angle for the pyrrole monomer obtained from the Newton diagram (Figure 2) assuming an ideally elastic collision is $\Theta_1 = 9.0°$ (dotted line in Figure 4a). Considering the finite angular spread of the beam of $\Delta\Theta \approx 1°$ (fwhm), the shift in the threshold angle to 8.2° would be more consistent with the measured angular distribution shape. This shift can be caused by an inelastic collision with an energy transfer of $\Delta E/E \approx 0.3$. This energy transfer turned out to agree also with the measured velocity distributions discussed below. In addition, from these velocity distributions, a similar amount of energy transfer was derived also for dimers. Therefore the threshold angles were consistently shifted for all the indicated neutral cluster sizes assuming the same energy transfer of $\Delta E/E \approx 0.3$. It ought to be mentioned that, as the distance between the threshold angles decreases with the increasing neutral cluster size n, also the shift due to the collision inelasticity becomes smaller so that it is only significant for the monomer and the dimer.

Figure 4b shows the corresponding angular distributions for clusters produced in Ar expansion. Because of the smaller cluster velocity in Ar with respect to He (see Table 1), the corresponding threshold scattering angles for the pure Py_n clusters are larger. The most striking difference with respect to the previous angular distributions is the sharp exponential drop of intensity that extends to significantly smaller scattering angles.[44] There is clearly no significant monomer fraction in the neutral beam that would be directly ionized to Py^+. This is in contrast to the He expansion, where the part of Py^+ ion signal at $\Theta > \Theta_2 = 4.1°$ can only be due to the direct neutral monomer ionization. Also the smaller clusters cannot be populated significantly in the beam. The monomer Py^+ fragment would originate from the Py_n $n \geq 5$ clusters if pure Py_n clusters were considered in the scattering (marked by dashed arrows in Figure 4b).

However, the data are best reproduced by the assumption that the mixed Ar_mPy_n clusters are produced in the Ar expansion and scattered from the secondary beams of He atoms. The measured Py_k^+ ions are the fragments of the A_mPy_n ionization. The deflection angles corresponding to Ar_8Py, Ar_8Py_2, and Ar_8Py_3 are 4.2°, 3.6°, and 3.1°, respectively (indicated by the solid arrows in Figure 4b), in very good agreement with the onset of intensities of the Py_k^+ fragment ions for $n = 1$, 2, and 3. Apparently, the Ar atoms evaporate during the ionization process.

To obtain the neutral cluster fragmentation probabilities, the angular distributions in He expansion were completed with TOF measurements for various fragment ions at various scattering angles. Figure 5 shows two examples of the measured TOF distributions of (a) Py^+ and (b) Py_2^+ fragments at the laboratory angle $\Theta = 3.3°$. Because this angle is larger than the trimer threshold angle $\Theta_3 = 2.8°$, only the neutral dimers can contribute to the Py_2^+ ion spectrum in Figure 5a. The gray arrows indicate the positions of the dimer peaks derived from the Newton diagram for forward and backward elastically scattered clusters.[45] Fitting with peaks fixed at these positions results in the spectrum (gray lines) noticeably broader than the experimental one. For inelastic collisions, the CM velocity of the scattered clusters, which corresponds to the radius of the scattering sphere, is smaller (see Figure 2), which results in a shift of the corresponding forward and backward peaks closer together. Transformation of about 30% of the collision energy

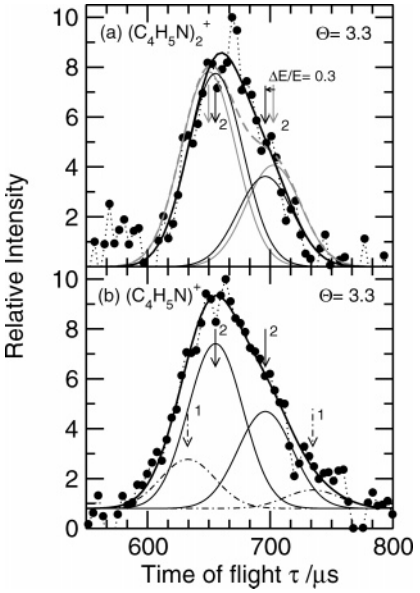

Figure 5. Measured TOF distributions of (a) dimer Py_2^+ and (b) monomer Py^+ fragment at the laboratory angle $\Theta = 3.3°$. The gray lines in (a) show the fit assuming the dimer TOF peak positions (indicated by gray arrows) given by ideally elastic scattering. The black line shows the fit considering the energy transfer in the collision of $\Delta E/E \approx 0.3$. For the monomer fragment spectrum (b), also neutral monomers had to be considered at this laboratory angle indicated by the dashed−dotted lines and arrows.

TABLE 2: Fragmentation Probabilities f_{nk}: $(C_4H_5N)_n \rightarrow (C_4H_5N)_k^+$

n	$k = 1$	2	3	4
2	0.78	0.22		
3	0.73	0.22	0.05	
4	0.62	0.29	0.09	0.00

into an internal excitation of the pyrrole cluster would result in the TOF peak positions indicated by the solid black arrows in Figure 5a and consecutively in the better fit (black line). This energy transfer is also consistent with the shift in the threshold scattering angles discussed above.

The TOF spectrum measured at the monomer ion signal, Figure 5b, was fitted with contributions from the neutral dimers (solid lines) and the monomers (dashed−dotted lines). Again the peak positions were determined from the Newton diagram by assuming the $\Delta E/E \approx 0.3$ energy transfer. Altogether, TOF spectra at five different angles between 2.2 and 4.2° were measured and fitted for contributions from neutral monomers through tetramers, checking for consistency between the various fits. In this way, the energy transfer of approximately $\Delta E/E \approx 0.3 \pm 0.1$ in inelastic collisions could be confirmed and the contributions from the various neutral cluster sizes to the various fragment ion signals at the given angles were determined.

Next, the cluster fragmentation can be obtained from the neutral cluster contributions to the ionic fragment TOF spectra. The resulting fragmentation probabilities f_{nk} of a neutral cluster size n to a fragment ion size k obtained for n, $k = 1-4$, are summarized in Table 2. Seventy-eight percent of the neutral dimers dissociate to Py^+ upon ionization, and 22% remain as Py_2^+ ions. Neutral trimers dissociate to the Py^+ ion from 73%, 22% dissociate to the dimer ion Py_2^+, and 5% remain as Py_3^+ ions. Sixty-two percent of neutral tetramers dissociate to the Py^+ ion, 29% to the Py_2^+ ion, 9% to the Py_3^+ ions, and there is no indication for the parent Py_4^+ ions.

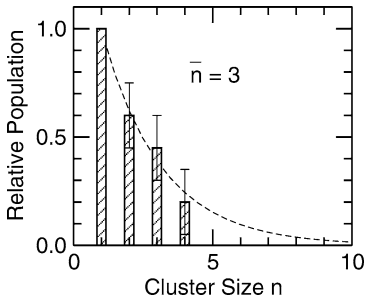

Figure 6. Neutral cluster size distribution evaluated from the measured scattering experiment of pyrrole clusters produced in He expansions deflected from He atom beam. Relative abundances of neutral cluster sizes up to the tetramer could be obtained. The distribution was fitted by exponential dependence (dashed line). The corresponding mean cluster size was $\bar{n} = 3$.

Once the fragmentation probabilities were obtained, the relative populations of the neutral cluster sizes n can be derived and subsequently the mean neutral cluster size $\bar{n}$ can be evaluated as an important byproduct of the present study, relevant for other experiments with Py clusters.[21] Integrating the eq 1 from $\Theta = 0°$ to the threshold angle Θ_n and using the normalization of the differential cross section $\sigma_n(\Theta)$, $\int_0^{\Theta_n} \sigma_n(\Theta)\, d\Theta = 1$, we obtain

$$\rho_n \propto \frac{I_n}{C_n f_{nk}} \tag{2}$$

To evaluate the integrals I_n, we use the measured angular distribution of the monomer ion $S_1(\Theta)$

$$S_1(\Theta) = \sum_{n=1}^{n_{max}(\Theta)} N_{n1}(\Theta) \tag{3}$$

where $n_{max}(\Theta)$ is the maximum cluster size scattered to the angle Θ. The relative contributions to the $S_1(\Theta)$ signal from the various neutral cluster sizes n were evaluated from the fitted TOF spectra at the measured angles Θ.

To determine the relative abundances proportional to the density ρ_n of neutral clusters of size n, the ionization cross section C_n is needed, eq 2. For larger clusters, the estimate of C_n being proportional to the geometrical cross section $C_n \propto n^{2/3}$ is generally used. Because we deal with rather small clusters, other estimates have been also used, e.g., $C_n = C_1 =$ const as the lower limit and $C_n \propto n$ as the upper limit. The scatter in the obtained ρ_n values using the different C_n estimates is included in the error bars in Figure 6.

The evaluated relative abundance of the neutral cluster sizes up to $n = 4$ are shown by the bars in Figure 6. For the small clusters, an exponential decrease of the abundances with the cluster size n can be assumed.[50] The dashed line in Figure 6 shows the exponential fit, which yields the mean cluster size of $\bar{n} = 3$.

4. Electronic Structure Calculations

A. Pyrrole Clusters. The energetics of the various fragmentation processes of small pyrrole clusters, obtained by the calculations described above, is depicted in Table 3. Optimized geometries both for the neutral clusters and for the ionic species are shown in Figure 7. Comparison between MP2 and DFT methods shows good agreement. The DFT method is known to suffer less from both the spin contamination[51] and the basis set superposition problem. This can be also seen in Table 3. The

TABLE 3: Energetics for Ionization and Fragmentation Processes of Pyrrole, Pyrrole Dimer, and Pyrrole Trimer[a]

process	DFT	MP2
(1) $(C_4H_5N) \rightarrow (C_4H_5N)^+$	8.20	8.04
(2) $(C_4H_5N)_2 \rightarrow (C_4H_5N)_2^+$	7.59	7.68
(3) $(C_4H_5N)_3 \rightarrow (C_4H_5N)_3^+$	7.59	7.90
(4) $(C_4H_5N)_3 \rightarrow (C_4H_5N)_2 + (C_4H_5N)$	0.36 (0.042)	0.87 (0.31)
(5) $(C_4H_5N)_2 \rightarrow (C_4H_5N) + (C_4H_5N)$	0.16 (0.022)	0.387 (0.15)
(6) $(C_4H_5N)_3^+$ (opt) $\rightarrow (C_4H_5N)_2^+ + (C_4H_5N)$	0.43 (0.03)	0.47 (0.174)
(7) $(C_4H_5N)_3^+$ (FC) $\rightarrow (C_4H_5N)_2^+ + (C_4H_5N)$	0.045 (0.04)	0.21 (0.288)
(8) $(C_4H_5N)_3^+$ (opt) $\rightarrow (C_4H_5N)^+ + (C_4H_5N)_2$	1.19 (0.025)	1.22 (0.16)
(9) $(C_4H_5N)_3^+$ (FC) $\rightarrow (C_4H_5N)^+ + (C_4H_5N)_2$	0.81 (0.037)	0.94 (0.28)
(10) $(C_4H_5N)_2^+$ (opt) $\rightarrow (C_4H_5N)^+ + (C_4H_5N)$	0.92 (0.03)	1.14 (0.22)
(11) $(C_4H_5N)_2^+$ (FC) $\rightarrow (C_4H_5N)^+ + (C_4H_5N)$	0.60 (0.02)	0.58 (0.13)

[a] Energies in eV are calculated at DFT/B3LYP level and at PMP2 level at UMP2 optimized geometries. 6-31+g* basis set is used for all the calculations. Energies are calculated without the basis set superposition error (BSSE). BSSE is shown in parentheses. Opt stands for optimized geometry in the ionized state, FC denotes ground-state optimal geometry.

figures presented here are therefore showing DFT structures and also the further discussion is based on DFT results unless stated otherwise. It should be, however, noticed that DFT methods with approximate functionals should be used with highest possible care because of the self-interaction error. This problem is typically much enhanced for systems with an odd number of electrons.[52] The problem in our case is manifested by an artificial charge delocalization for the DFT method at large intermolecular distances. Therefore, the results have always to be compared with results of methods that do not suffer from this error, in our case, the PMP2 method.

The ground-state structure of a pyrrole dimer has been previously estimated both experimentally[5] and theoretically.[6−8] Clusters up to four pyrrole units have been studied more recently.[9] Pyrrole clusters are bound predominantly by electrostatic interaction even though the dispersion interaction plays an important role. The characteristic feature for the global minima of small pyrrole clusters is the N−H bond of one pyrrole molecule pointing toward the ring plane of other pyrrole unit. Thus, for the pyrrole dimer, there is one free N−H bond, while for the trimer and tetramer, the structures are of cyclic type, with three or four hydrogen bonds. The dissociation energy of the pyrrole dimer (Table 3) has been estimated as 0.16 (0.39) eV at DFT (MP2) level. The estimated experimental value is 0.3 eV.[5] The energy for dissociating one pyrrole unit from the trimer is 0.36 (0.87) eV. The energies reported above do not include the basis set superposition correction. The basis set superposition correction for the process 5 (dimer dissociation) is 0.022 (0.15) eV, and for the process 4 (trimer dissociation) 0.042 (0.31) eV (DFT/MP2). The first value is for the DFT/B3LYP method with a 6-31+g* basis, while the value in parentheses refers to the MP2 method with the same basis. It is seen that the DFT method suffers much less from the BSSE than the MP2 method. Considering BSSE correction leads to a good agreement between DFT and MP2 dissociation energies values. As noticed in ref 9, the formation of pyrrole clusters shows certain cooperativity effects.

The calculated vertical ionization potential for the monomer (8.20 eV for DFT, 8.04 eV for MP2 method) is in an excellent agreement with the experimental value of 8.2 eV.[53] The ionization potential decreases for the dimer and the trimer. After the ionization, the pyrrole monomer undergoes only small changes both in energy and in the geometry, see Figure 7a. The length of the CC bond opposite to the nitrogen atom changes from 1.43 Å (indicating dominantly single bond character) to 1.38 Å (getting partially double bond character) while the CC bond closer to the nitrogen atom gets longer (1.4 Å instead of 1.38 Å in the ground state). The energy change accompanying this intramolecular relaxation is less than 0.2 eV.

The dimer minimum is already geometrically significantly different from the ground-state geometry. The dimer ion forms a stacked structure, with the two pyrrole units being to a certain degree shifted (parallel-displaced structure) as indicated in Figure 7b. The nitrogen atoms are pointing in opposite directions, but a stacked structure with parallel nitrogen orientations is only 0.07 eV above the global minimum. The potential energy surface for the intermolecular motion is rather shallow. The relaxation in the ionic state thus releases an energy of about 0.3 eV, which is less than the binding energy of the dimer ion (0.92 eV, see process 10 in Table 3). The ionization in this case does not deposit enough energy into the dissociative mode. The threshold ionization then does not lead to a direct dissociation of the dimer ion. Note that the positive charge is delocalized uniformly in the pyrrole dimer cation, i.e., both subunits have the charge of 0.5e. This can be directly seen from the population analysis, and the fact is also reflected in the structure of the pyrrole subunits in the dimer ion. The bond lengths for these pyrrole molecules are in between those found in the pyrrole ion and neutral pyrrole. The charge delocalization in this case is not an artifact of the approximate density functional. The same delocalization is observed with the MP2 wavefunction. The intermolecular distance between the two pyrrole units is approximately 3 Å. As we increase this distance, the charge will localize on one of the pyrrole units. Note that the DFT/B3LYP method is unable to describe this localization (which is seen for distances between 6 and 7 Å). During the process of ionization, the intermolecular distance has to significantly shorten from 4.1 Å in the ground-state dimer to 3.25 Å in the ionized molecule.

The pyrrole trimer cation has already richer conformational space. In Figure 7c, three pyrrole trimer structures are shown: the ground-state minimum (i.e., Franck−Condon point), the local minimum obtained by minimization from the Franck−Condon point, and the lowest minimum found. It is immediately seen that, after the ionization, a stacked dimer ion core is formed. The third pyrrole unit serves mostly as a "solvent" for the dimer core. After some further rearrangement, the system reaches the global minimum. Here, the process of a "dimer core solvation" is completed. Note however that the global minimum is close in energy to other possible structures, e.g., a stacked complex that is energetically less than 0.15 eV higher in energy than the global minimum at both DFT and MP2 levels. Ion core formation can be viewed by an inspection of the intermolecular distances. For the ion core, the distance between molecule's center of mass decreases from 4.33 to 3.31 Å, similarly to the dimer ion. The third molecule appears to be farther away from both pyrrole units. The picture of the pyrrole trimer cation as a pyrrole solvated ion (dimer) core is also supported by a population analysis. For the global minimum of the trimer radical cation, some 95% of the excess positive charge is localized on the dimer core; for the local minimum, this quantity is 90% of the excess charge. Formation of a solvated dimer core can be also seen from geometries of the pyrrole trimer subunits: the dimer core clearly has bond lengths found for the dimer ion, while the third excluded unit has a geometry of a ground-state molecule. The reaction energy for the fragmentation of a pyrrole trimer ion into a pyrrole dimer ion and a neutral monomer is 0.43 eV. Almost the same energy is, however,

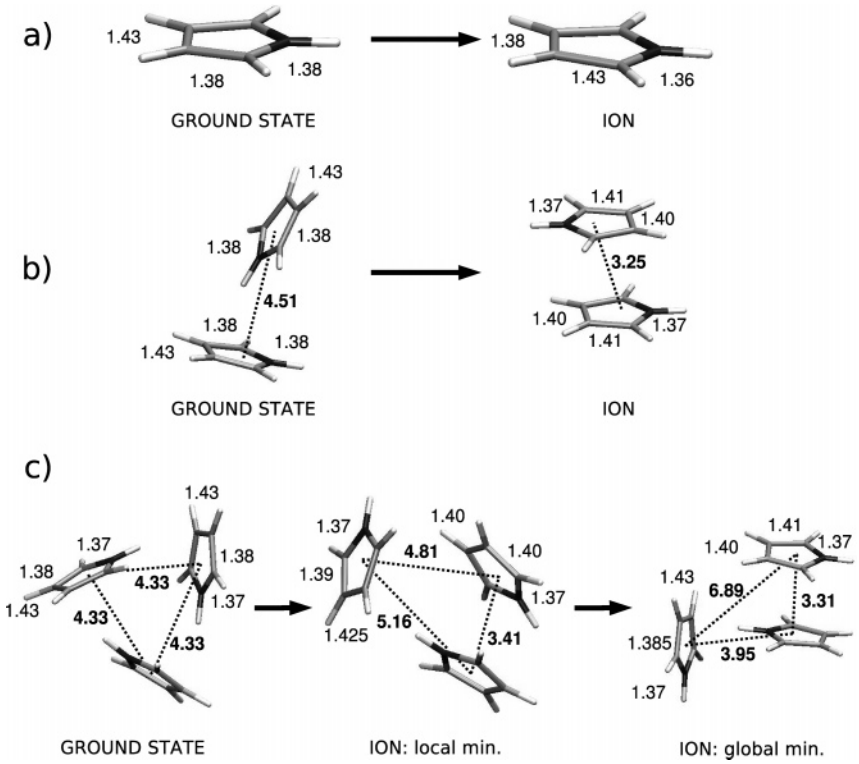

Figure 7. Calculated geometries of pyrrole monomer, dimer, and trimer and of corresponding ionized species. The geometries have been optimized at DFT level with a B3LYP functional and 6-31+g* basis set.

deposited into the vibrational modes during the relaxation in the ionic state. As can be seen from Figure 7c, after the ionization, the dissociative mode is immediately triggered. Even energies that are only slightly higher than the threshold ionization energies can then lead to the cluster fragmentation. There is also another dissociation process available in which a charged pyrrole molecule and a neutral pyrrole dimer are formed (processes 8 and 9 in Table 3). This channel is, however, energetically significantly higher than the dissociation into a neutral monomer and dimer core. The reason is that the binding energy between pyrrole molecules is much higher for the charged dimer than for the neutral species. Note also that, while cooperativity effect has been observed for the pyrrole clusters in the ground state, negative cooperativity is present in the charged complexes. This results in the nonmonotonic evolution of the ionization potential with the cluster size.

While pyrrole trimer cations have not been to our best knowledge studied, significant attention has been paid to the behavior of charged clusters of other aromatic molecules, in particular, benzene.[4,28] Pyrrole complexes differ to some extent from the benzene clusters in the ground state. This is caused by the different character of the bonding, with benzene being dominated by dispersion interactions and pyrrole by electrostatic terms. It is, however, interesting that the behavior of pyrrole cluster ions seems to be highly similar to their benzene analogues. In the benzene case, too, the dimer core is likely to form with the other benzene molecule solvating this core.

B. Pyrrole−Ar Clusters. Complexes of a pyrrole molecule with an argon atom has been studied previously via microwave spectroscopy.[34] The global minimum of this complex corresponds to an argon atom being almost directly above the midpoint between the two ring carbons adjacent to the N atom; the distance of the argon from the center of mass is 3.55 Å. On the basis of the measured structural parameters, the dissociation energy D_0 of this complex has been estimated to be about 37 meV (300 cm^{-1}). Because this complex is dominantly bound by the dispersion interaction, we have used MP2 and CCSD(T) methods to study this system. Basis set saturation is of major importance in this case. We have performed the geometry optimization using the aug-cc-pVDZ basis set. Optimization has been performed on the MP2 level, and basis set superposition correction has not been considered during the optimization procedure. For the optimized geometry, the basis set superposition error has been evaluated. A larger fraction of the correlation energy has been also included via recalculating the dissociation energies with the CCSD(T) method. Furthermore, the basis set has been augmented by a set of midpoint functions consisting of 3 s, 3 p, and 2 d functions. These functions have been placed in the middle of the line connecting the pyrrole center-of-mass with the argon atom. Exponents of s and p functions are 0.9, 0.3, and 0.1, exponents of d functions are set to 0.6 and 0.2. Adding the midbond functions leads to a rapid convergence of dispersion-based intramolecular energy. The CCSD(T) method with the aug-cc-pVDZ basis set augmented with the midbond function yields then highly accurate results for these complexes.[54,55] Results of our calculations for a neutral pyrrole−argon complex are in a good agreement with the experiment, the minimum was localized as that found by Bohn et al.,[34] with the argon center of mass distance 3.43 Å. The dissociation energy D_e of this complex (see Table 4) was found to be 42.0 meV at the CCSD(T) level. In addition to the global minimum, there is also a secondary minimum lying in the pyrrole molecule plane. This minimum is about 12 meV above the global minimum. The dissociation energy for the pyrrole cation−argon complex has been calculated to be 64.5 meV. It is thus stabilized by 22.4 meV more than the neutral species. These results are to a large extent similar to those obtained for the benzene−argon complex.[35,54] The dissociation energies are somewhat smaller for pyrrole than for benzene. This is expected because pyrrole has only five heavy atoms compared to six in benzene. The global minimum of the ionic complex still corresponds to a configuration with the argon atom located above the pyrrole

TABLE 4: Dissociation Energies D_e in meV (Values in cm^{-1} Given in Parenthesis) for Pyrrole−Argon Neutral Complex and Its Ion[a]

species	MP2	CCSD(T)
$C_4H_5N\cdots Ar$	56.9 (459)	42.0 (339)
$(C_4H_5N\cdots Ar)^+$	75.0 (605)	64.5 (520)

[a] Energies are calculated at the MP2 and CCSD(T) levels with aug-cc-pVDZ basis set augmented with a set of diffuse functions placed in the mid-bond region. Basis set superposition error is included.

plane. However, the excited-state van der Waals potential energy surface is more isotropic, and the energy for the argon atom placed in the pyrrole plane is higher by only some 1.2 meV than the global minimum.

5. Discussion

From the scattering experiments, the fragmentation probabilities of Py_n clusters, $n = 1-4$, were obtained and summarized in Table 2. The analysis has been fully size-selective. The major ionic fragment is the monomer: 78% of the neutral dimers, 73% of the trimers, and 62% of the tetramers fragment to Py^+. The other significant fragment populated by more than 20% is Py_2^+. The trimer ion Py_3^+ is generated by fragmentation of less than 10% of the neutral trimers and tetramers. The fragmentation probability distribution reflects the distribution of energy in the molecule upon electron impact. In principle, this distribution can be extracted from the fragmentation probabilities using energetical considerations, as has been done for charged argon clusters.[38] In the Ar case, it was concluded that on average about 2 eV (at most 6 eV) from the initial 70 eV energy of the ionizing electron remains deposited in the cluster after ionization. This conclusion has been confirmed by recent calculations that take into account all relevant electronic states of the ion and their couplings.[56]

It is generally accepted that the electron first ionizes the cluster and the subsequent fragmentation is caused by the energy released into the system as the clusters change from their neutral to their ionic equilibrium structure.[56] The combination of ab initio calculations presented above with the measured fragmentation probabilities suggests that the deposited energy distribution is not significantly different for the present case. The pyrrole dimer ion dissociation energy is approximately 1 eV, for the pyrrole trimer ion, it is about 0.4 eV, and thus the total binding energy for the trimer is ~1.4 eV. Dissociation energies for dissociating a monomer unit from the larger clusters have not been calculated, but their values can be expected to be somewhat lower than the 0.4 eV for the trimer. From the fragmentation probability $f_{21} = 0.78$, it follows that approximately 80% of ionized clusters have an energy larger than 1 eV, which leads to the dimer dissociation. Only a few percent of ionized clusters have an energy below the dissociation energy of the trimer ~0.4 eV because $f_{33} = 0.05$. Thus the distribution of the energy deposited into the cluster upon ionization can be expected to peak at around 1 eV. The tetramer is expected to fragment even after ionizing near the threshold because the ground-state and ionic minima are quite different, which is in agreement with the observed $f_{44} \approx 0$.

Fragmentation probabilities are thus fully in accord with the picture of pyrrole clusters as it emerges from the ab initio calculations. This is a strongly bound dimer ion core with the other pyrrole molecules just solvating this core. Pyrrole units can also switch their identities, possibly leading to a charge transfer via a hopping mechanism. Pyrrole clusters in this respect resemble benzene clusters where the formation of a dimer ionic core is strongly supported by different experiments and a series of theoretical calculations.[29]

The distribution of energy deposited in the cluster upon the electron impact also explains the observed mass spectra in Figure 3. They exhibit an interesting tendency of the cluster to create ionic fragments composed of the whole number of molecules Py_k^+. In contrast, the pyrrole monomer mass spectrum[18,57] exhibits a group of fragments around mass 40 amu and smaller ones at 28 amu.[58] This indicates that, upon electron impact ionization, the pyrrole molecule in the cluster does not fragment as much as the pyrrole molecule alone. This brings an upper bound to the energy deposited in the molecule. As follows from both the experiment[18] and theoretical calculations,[59] an energy exceeding 4 eV is needed to cause the isolated molecule to fragment. This energy is apparently to some extent available after the electron impact ionization. On the other hand, the molecular ion is still the most abundant ion.

Because only a small fraction of the electron kinetic energy is deposited into the cluster, upon ionization, a comparison with photofragmentation experiment of Rennie et al.[18] can be made. By comparing the photoabsorption spectra with the mass spectra in ref 18, the maximum amount of energy deposited into the molecule can be deduced. Ionization with 12 eV energy photons led almost exclusively to the parent Py^+ ion, while photoionization at 14 eV already produced a significant fragmentation such that Py^+ ion was much less abundant than the fragments with masses 41 and 40 amu. Thus an energy slightly less than 13 eV would be roughly consistent with the measured mass spectrum. This leaves less than 5 eV for the excitation of the molecule, considering the 8.2 eV ionization potential. Note that the complete agreement between the photodissociation and the mass spectra cannot be achieved, which is probably due to the different timescales of the experiments. Yet the present comparison yields a reasonable estimate of the maximum energy deposited into the molecule upon electron impact ionization.

This conclusion, that no more than 5 eV is present in the molecule, is also in full agreement with our mass spectra of pyrrole clusters. Dissociation of clusters rather than the individual molecules is the energetically preferred fragmentation route because the required energy is much lower. This fragmentation up to the monomer ion requires at least 1 eV for the dimer ion, 1.4 eV for the trimer, and slightly more for the larger cluster ions. The remaining energy is then not sufficient to fragment the molecular ion, i.e., this energy has to be below 3 eV (considering again the photoionization picture from ref 18). These ~3 eV added to the ~1−2 eV required to fragment the ionic clusters above is consistent with less than 5 eV deposited in the molecule.

It should be stressed that only a small fraction of the 70 eV of the ionizing electron kinetic energy is deposited into cluster: only about 1 eV above the ionization threshold. In fact, the electron impact ionization of the cluster is quite gentle despite the large kinetic energy of the electron. Thus we do not expect a significant dependence of the pyrrole cluster fragmentation pattern on the electron energy in our experimentally accessible region between 30 and 100 eV. We have explored this region for Ar clusters, where the measured Ar_n^+ mass spectra exhibited little dependence on the ionizing electron energy (except for the overall intensity of the spectra), suggesting a similar fragmentation pattern for all the explored energies in complete agreement with earlier studies.[42] Because a very similar amount of energy is deposited into the Py_n cluster upon ionization as for Ar_n, there is also little electron energy dependence expected for the Py_n clusters.

The tendency of pyrrole clusters to fragment the whole molecules is not ubiquitous for molecular clusters. The mass spectra of ethylene[60] or carbonylsulfide[61] clusters exhibit a whole variety of fragments as a result of fragmentation of the ionized molecule and subsequent intracluster ion−molecule reactions of the ionic fragments. On the other hand, some hydrogen-bonded clusters such as ammonia,[62] methyl glycolate,[63] or methyl lactate[64] are dominated by the protonated clusters M_nH^+ (M = the corresponding molecule). Thus the pyrrole spectrum dominated by Py_n^+ fragments represents a peculiar case that can be traced back to the special bonding between the pyrrole molecules discussed in the theoretical part. Notice that this feature can be also found in ionized benzene clusters.[4]

The generation of clusters of helium with pyrrole molecules is quite improbable under our experimental conditions.[32] In Ar expansions, on the other hand, mixed clusters Ar_mPy_n can be generated. However, the absence of mixed $Ar_mPy_k^+$ ions in the spectrum, Figure 3b, indicates that the mixed neutral clusters *shake off* all the Ar atoms upon ionization to generate the bare Py_k^+ fragments. In the measured angular distributions, the onset of the Py_k^+ ion signals, $k = 1, 2, 3$, best correspond to the scattering of Ar_8Py_k neutral clusters. It should be mentioned that the angular distance between the threshold angles ranges between approximately 0.5° for Ar_mPy_1 and 0.3° for Ar_mPy_3 for $m = 6$ and 10, respectively. Therefore, a distribution of number of Ar atoms can be attached to the pyrrole clusters Ar_m-Py_n, the mean number of which can be estimated as $\bar{m} = 8$. In addition, assuming that pyrrole clusters fragment after Ar evaporation in a similar way as the pure pyrrole clusters, the mean number $\bar{n} = 4$ of Py molecules in the Ar_mPy_n cluster can be also estimated from comparison of the mass spectra in parts a and b of Figure 3.

Dissociation of Ar from $(Py{\cdot}Ar)^+$ and $(Py{\cdot}Ar_2)^+$ complexes has been observed.[36,65] It should be noted that the Ar−Py bond is significantly weaker than the Py−Py bond. According to our calculations, argon is bound to a pyrrole molecule by an energy of approximately 42 meV in the ground state and 64 meV in the ionic state. It has been argued above that about 1 eV (5 eV at most) energy is deposited into the cluster in the ionization process. In the pure Ar_n clusters, 1 eV of energy corresponds to the total binding energy of about 21 Ar atoms.[66] Thus it is feasible that the mixed cluster Ar_mPy_n with the mean number $\bar{m} = 8$ atoms ejects all the Ar atoms after the ionization producing the observed Py_k^+ ions.

It is also worth mentioning at this point that Dauster and Suhm[67] have seen spectroscopic fingerprints of pyrrole clusters up to tetramer embedded in large Ar clusters produced in their supersonic slit expansions with Ar. Indeed, their slit expansion is quite different from our nozzle, nevertheless, in previous experiments,[63,64] vibrational spectra of clusters produced in supersonic slit expansions were compared to the spectra of clusters produced in a nozzle identical with the present one. The analogy of the spectra suggested that similar species are produced. Thus the above-mentioned experiment[67] also support the generation of the mixed Ar_mPy_n species in our experiment.

Finally, the analysis of the scattering experiment in He expansion revealed some energy transfer in the collision of He atoms with the clusters. Because the collision energy in the present experiment with He expansion is 106 meV, the above-derived energy transfer $\Delta E/E \approx 0.3 \pm 0.1$ means approximately 32 ± 11 meV transferred by the He atom into the internal excitation of the pyrrole clusters in the collision. It should be noted that this energy is quite low compared to the excitation brought in the cluster by the ionization discussed above, and therefore it can be neglected in the cluster fragmentation process.

6. Conclusions

Small pyrrole clusters have been produced in expansions of Py molecules seeded in helium. From the analysis of a scattering experiment with the secondary beam of He atoms, the fragmentation probabilities of Py_n, $n = 2-4$, upon 70 eV electron impact ionization to Py_k^+, $k = 1-4$, were evaluated. The main fragment channels are the monomer ion Py_1^+ with about 70% and the dimer ion Py_2^+ with about 24%. The neutral trimer and tetramer decay by more than 90% to these products. We note that only cluster ions of intact monomer units are observed, in contrast to the behavior of the neutral monomer and many other hydrogen-bonded clusters. To rationalize the observed results, we have calculated structures and energetics of small pyrrole clusters (monomer to trimer) and of their ions using DFT and PMP2 methods with a 6-31+g* basis. The analysis of the ab initio calculations has shown that the cluster ions are formed by a dimer ionic core that is solvated by neutral pyrrole molecules. The pyrrole dimer ion is bound by about 1 eV while adding subsequent pyrrole molecules leads to a smaller decrease in energy (about 0.4 eV for trimer). The analysis of the experiment also delivered the neutral cluster size distribution with the mean cluster size $\bar{n} = 3$ as a byproduct of these experiments relevant for other studies.[21]

In expansions of Py molecules seeded in Ar, larger mixed Ar_mPy_n clusters are produced. The onsets of Py_k^+ fragment ions coincide with the scattering of Ar_mPy_n neutral clusters with the mean number of Ar atoms $\bar{m} = 8$. This suggests that all Ar atoms are evaporated upon ionization. The mean number of Py molecules in the mixed Ar_mPy_n clusters has been determined $\bar{n} = 4$. Thus the total neutral cluster size $\bar{m} + \bar{n} = 12$ is much larger than in the He expansions, where $\bar{n} = 3$. The formation of mixed argon−pyrrole clusters has been discussed in the light of electronic structure calculations of pyrrole−argon cluster in the ground and ionic states with a highly accurate CCSD(T)/aug-cc-pVDZ+ midbond level. The calculated dissociation energies of 42 meV for the ground-state complex and 64 meV for the ionized species suggest that the argon atoms can rapidly evaporate after the ionization.

The combined analysis of fragmentation probabilities together with the ab initio calculations has shown that ionized pyrrole clusters are formed by a dimer ionic core, which is solvated by neutral pyrrole molecules. This arrangement leads to the strong fragmentation of the neutral trimer and tetramer to the dimer and monomer ion. From the experiment and the calculations, we have also been able to estimate the distribution of energy deposited in the cluster after the electron impact. In agreement with previous estimates on different systems, the deposited energy with a maximum above 1 eV and less than 5 eV in the tail is expected.

The behavior of pyrrole clusters and pyrrole−argon clusters has been compared to the much more studied benzene clusters. Even though the nature of interactions in the ground-state pyrrole and ground-state benzene clusters is to a certain extent different, the behavior of ionized clusters is quite similar both for pure clusters and clusters with argon atoms. In general, pyrrole clusters with the active NH bond can serve as a prototypical model for studying interactions between biomolecules.

Acknowledgment. We thank V. Kresin for valuable discussions and I. Dauster and M. A. Suhm for sharing their unpublished results. Support by the special program "Nano-

technology for Society" of the Czech Academy of Sciences KAN400400461, and by the Grant Agency of the Czech Republic 203/06/1290 is gratefully acknowledged. M.F. acknowledges a special J.E. Purkyne fellowship of the Czech Academy of Sciences, and P.S. the postdoctoral grant of Grant agency of the Czech Republic 203/07/P449. V. Profant acknowledges the university grant 8113-10/257852.

References and Notes

(1) Jena, P.; Castleman, A. W. *Proc. Nat. Acad. Sci. U.S.A.* **2006**, *103*, 10560.

(2) Hobza, P.; Selzle, H.; Schlag, E. *Chem. Rev.* **1994**, *94*, 1767.

(3) Dermota, T.; Zhong, Q.; Castleman, A. W. *Chem. Rev.* **2004**, *104*, 1861.

(4) Rusyniak, M. J.; Ibrahim, Y. M.; Wright, D. L.; Khanna, S. N.; El-Shall, M. S. *J. Am. Chem. Soc.* **2003**, *125*, 12001.

(5) Columberg, G.; Bauder, A. *J. Chem. Phys.* **1997**, *106*, 504.

(6) Stefov, V.; Pejov, L.; Soptrajanov, B. *J. Mol. Struct.* **2003**, *649*, 231.

(7) Park, H.; Lee, S. *Chem. Phys. Lett.* **1999**, *301*, 487.

(8) Lukes, V.; Breza, M.; Biskupic, S. *Theor. Chem. Acc.* **1999**, *101*, 319−324.

(9) Gómez-Zavaglia, A.; Fausto, R. *J. Phys. Chem. A* **2004**, *108*, 6953.

(10) Blank, D. A.; North, S. W.; Lee, Y. T. *Chem. Phys.* **1994**, *187*, 35.

(11) Cronin, B.; Nix, M. G. D.; Qadiri, R. H.; Ashfold, M. N. R. *Phys. Chem. Chem. Phys.* **2004**, *6*, 5031.

(12) Wei, J.; Kuczmann, A.; Riedel, J.; Renth, F.; Temps, F. *Phys. Chem. Chem. Phys.* **2003**, *5*, 315.

(13) Papadakis, V.; Kitsopoulos, T. N. *Rev. Sci. Instrum.* **2006**, *77*, 083101.

(14) Wei, J.; Riedel, J.; Kuczmann, A.; Renth, F.; Temps, F. *Faraday Discuss.* **2004**, *127*, 267.

(15) van den Brom, A. J.; Kapelios, M.; Kitsopoulos, T. N.; Nahler, N. H.; Cronin, B.; Ashfold, M. N. R. *Phys. Chem. Chem. Phys.* **2005**, *7*, 892.

(16) Lippert, H.; Ritzel, H.-H.; Hertel, I. V.; Radloff, W. *ChemPhysChem* **2004**, *5*, 1423.

(17) Barbatti, M.; Vazdar, M.; Aquino, A. J. A.; Eckert-Maksić, M.; Lischka, H. *J. Chem. Phys.* **2006**, *125*, 164323.

(18) Rennie, E. E.; Johnson, C. A. F.; Parker, J. E.; Holland, R. F. D. M. P.; Shaw, D. A. *Chem. Phys.* **1999**, *250*, 217.

(19) Cauet, E.; Dehareng, D.; Lievin, J. *Adv. Quantum Chem.* **2006**, *110*, 9200−9211.

(20) Crespo-Hernandez, C. E.; Cohen, B.; Hare, P. M.; Kohler, B. *Chem. Rev.* **2004**, *104*, 1977.

(21) Poterya, V.; Profant, V.; Fárník, M.; Slavíček, P.; Buck, U. *J. Chem. Phys.* **2007**, 064307.

(22) Rubio-Lago, L.; Zaouris, D.; Sakellariou, Y.; Sofikitis, D.; Kitsopoulos, T. N.; Wang, F.; Yang, X.; Cronin, B.; Devine, A. L.; King, G. A.; Nix, M. G. D.; Ashfold, M. N. R.; Xantheas, S. S. *J. Chem. Phys.* **2007**, 064306.

(23) Sinnokrot, M. O.; Sherrill, C. D. *J. Phys. Chem. A* **2006**, *110*, 10656.

(24) Badger, B.; Rockleh, B. *Nature* **1968**, *219*, 263.

(25) Krause, H.; Ernstberger, B.; Neusser, H. J. *Chem. Phys. Lett.* **1991**, *184*, 411.

(26) Ohashi, K.; Nishi, N. *J. Chem. Phys.* **1998**, *109*, 3971.

(27) Hiraoka, K.; Fujimaki, S.; Aruga, K.; Yamabe, S. *Chem. Phys.* **1991**, *95*, 8413.

(28) Miyoshi, E.; Ghosh, T. K. *Chem. Phys. Lett.* **2000**, *323*, 434−440.

(29) Mine, M.; Mori, H.; Ogata, M.; Tanaka, S.; T, T.; Miyoshi, E. *Chem. Phys. Lett.* **2007**, *438*, 157.

(30) Saigusa, H.; Lim, E. C. *J. Phys. Chem.* **1994**, *98*, 13470.

(31) Braun, J.; Neusser, H.; Hobza, P. *J. Phys. Chem. A* **2003**, *107*, 3918.

(32) Such clusters were generated with benzene in expansions of 70 bar through an 0.8 mm diameter orifice.[33]

(33) Lee, S.; Chung, J. S.; Felker, P. M.; López-Cacheiro, J.; Fernandez, B.; Koch, H. *J. Chem. Phys.* **2003**, *119*, 12956.

(34) Bohn, R. K.; Hillig, K. W.; Kuczkowski, R. L. *J. Phys. Chem.* **1989**, *93*, 3456.

(35) Sampson, R. K.; Lawrance, W. D. *Aust. J. Chem.* **2003**, *56*, 275.

(36) Krause, H.; Neusser, H. J. *J. Chem. Phys.* **1993**, *99*, 6278.

(37) Koch, H.; Fernandez, B.; Makarewicz, J. *J. Chem. Phys.* **1999**, *111*, 198.

(38) Lohbrandt, P.; Galonska, R.; Kim, H. J.; Lauenstein, M. S. C.; Buck, U. In *Atomic and Molecular Beams. The State of the Art 2000*; Campargue, R., Ed. Springer: Berlin, 2001; p 623.

(39) Buck, U. *J. Phys. Chem. A* **2002**, *106*, 10049.

(40) Baumfalk, R.; Buck, U.; Frischkorn, C.; Gandhi, S. R.; Lauenstein, C. *Ber. Bunsen-Ges. Phys. Chem.* **1997**, *101*, 606.

(41) Because the pyrrole tends to polymerize at elevated temperatures and also to assure the pyrrole purity, the pyrrole in the reservoir was exchanged frequently.

(42) Buck, U.; Meyer, H. *J. Chem. Phys.* **1986**, *84*, 4854.

(43) Steinbach, C.; Fárník, M.; Buck, U.; Brindle, C. A.; Janda, K. C. *J. Phys. Chem. A* **2006**, *110*, 9108.

(44) Because the signals in Ar expansions are an order of magnitude larger than in He, this cannot be just an experimental artifact due to a low signal intensity.

(45) The lower resolution of the present apparatus does not allow one to fully resolve the individual peaks due to the contribution from the various neutral cluster sizes. Yet, in our previous paper on Kr_n fragmentation,[43] we have demonstrated that the analysis of the low-resolution results from the present apparatus yields essentially the same fragmentation probabilities as significantly better-resolved spectra from another molecular beam scattering machine.

(46) Schlegel, H. B. *J. Chem. Phys.* **1986**, *84*, 4530.

(47) Crespo-Hernandez, C. E.; Arce, R.; Ishikawa, Y.; Gorb, L.; Leszczynski, J.; Close, D. M. *J. Phys. Chem. A* **2004**, *108*, 6373.

(48) Frisch, M. J.; Trucks, G. W.; Schlegel, H. B.; Scuseria, G. E.; Robb, M. A.; Cheeseman, J. R.; Montgomery, J. A., Jr.; Vreven, T.; Kudin, K. N.; Burant, J. C.; Millam, J. M.; Iyengar, S. S.; Tomasi, J.; Barone, V.; Mennucci, B.; Cossi, M.; Scalmani, G.; Rega, N.; Petersson, G. A.; Nakatsuji, H.; Hada, M.; Ehara, M.; Toyota, K.; Fukuda, R.; Hasegawa, J.; Ishida, M.; Nakajima, T.; Honda, Y.; Kitao, O.; Nakai, H.; Klene, M.; Li, X.; Knox, J. E.; Hratchian, H. P.; Cross, J. B.; Bakken, V.; Adamo, C.; Jaramillo, J.; Gomperts, R.; Stratmann, R. E.; Yazyev, O.; Austin, A. J.; Cammi, R.; Pomelli, C.; Ochterski, J. W.; Ayala, P. Y.; Morokuma, K.; Voth, G. A.; Salvador, P.; Dannenberg, J. J.; Zakrzewski, V. G.; Dapprich, S.; Daniels, A. D.; Strain, M. C.; Farkas, O.; Malick, D. K.; Rabuck, A. D.; Raghavachari, K.; Foresman, J. B.; Ortiz, J. V.; Cui, Q.; Baboul, A. G.; Clifford, S.; Cioslowski, J.; Stefanov, B. B.; Liu, G.; Liashenko, A.; Piskorz, P.; Komaromi, I.; Martin, R. L.; Fox, D. J.; Keith, T.; Al-Laham, M. A.; Peng, C. Y.; Nanayakkara, A.; Challacombe, M.; Gill, P. M. W.; Johnson, B.; Chen, W.; Wong, M. W.; Gonzalez, C.; Pople, J. A. *Gaussian 03*, revision C.02; Gaussian, Inc.: Wallingford, CT, 2004.

(49) Boys, S. F.; Bernardi, F. *Mol. Phys.* **1970**, *19*, 553.

(50) Bobbert, C.; Schütte, S.; Steinbach, C.; Buck, U. *Eur. Phys. J. D* **2002**, *19*, 183.

(51) Baker, J.; Scheiner, A.; Andzelm, J. *Chem. Phys. Lett.* **1993**, *216*, 380.

(52) Mantz, Y. A.; Gervasio, F. L.; Laino, T.; Parrinello, M. *J. Phys. Chem. A* **2007**, *111*, 105.

(53) Willet, G. D.; Baer, T. *J. Am. Chem. Soc.* **1980**, *102*, 6774.

(54) Koch, H.; Fernandez, B.; Christiansen, O. *J. Chem. Phys.* **1998**, *108*, 2784.

(55) Slavicek, P.; Kalus, R.; Paska, P.; Odvarkova, I.; Hobza, P.; Malijevsky, A. *J. Chem. Phys.* **2003**, *119*, 2102.

(56) Bonhommeau, D.; Halberstadt, N.; Buck, U. *Int. Rev. Phys. Chem.* **2007**, *26*, 353.

(57) In *NIST Chemistry WebBook, NIST Standard Reference Database Number 69*; Linstrom, P. J., Mallard, W. G., Eds.; National Institute of Standards and Technology: Gaithersburg MD, June 2005; (http://webbook.nist.gov).

(58) The part of the spectrum corresponding to the monomer ion and masses below has been omitted from Figure 3. Because the signals and the backgrounds were much higher in this region, this part was studied in more detail using a different quadrupole high-Q head and a higher mass resolution. The results were in agreement with the mass spectra published in the literature.[57]

(59) Van der Hart, W. J. *Int. J. Mass Spectrom.* **2000**, *198*, 33.

(60) Buck, U.; Lauenstein, C.; Meyer, H.; Sroka, R. *J. Phys. Chem.* **1988**, *92*, 1916−1922.

(61) Buck, U.; Hobein, M.; Krohne, R.; Linnartz, H. *Z. Phys. D* **1991**, *20*, 181.

(62) Buck, U.; Lauenstein, C. *J. Chem. Phys.* **1990**, *92*, 4250.

(63) Fárník, M.; Steinbach, C.; Weimann, M.; Buck, U.; Borho, N.; Suhm, M. A. *Phys. Chem. Chem. Phys.* **2004**, *6*, 4614.

(64) Fárník, M.; Weimann, M.; Steinbach, C.; Buck, U.; Borho, N.; Adler, T. B.; Suhm, M. A. *Phys. Chem. Chem. Phys.* **2006**, *8*, 1148.

(65) Gascooke, J. R.; Lawrance, W. D. *J. Phys. Chem. A* **2000**, *104*, 10328.

(66) Naumkin, F. Y.; Wales, D. J. *Mol. Phys.* **1999**, *96*, 1295.

(67) Dauster, I.; Suhm, M. A. 2007, unpublished results.